EXPERIMENTAL CELL RESEARCH 313 (2007) 2204–2216

available at www.sciencedirect.com

ScienceDirect

www.elsevier.com/locate/yexcr

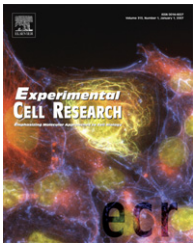

Review Article

# Towards a molecular description of intermediate filament structure and assembly☆

*David A.D. Parry*[a,1], *Sergei V. Strelkov*[b,1], *Peter Burkhard*[c], *Ueli Aebi*[d], *Harald Herrmann*[e,*]

[a]*Institute of Fundamental Sciences, Massey University, Private Bag 11-222, Palmerston North, New Zealand*
[b]*Department of Pharmaceutical Sciences, Catholic University of Leuven, Herestraat 49 bus 822, B-3000 Leuven, Belgium*
[c]*Institute of Materials Science, University of Connecticut, 97 North Eagleville Road, Storrs, CT 06269-3136, USA*
[d]*Institute of Structural Biology, Biozentrum, University of Basel, Klingelbergstrasse 70, CH-4056 Basel, Switzerland*
[e]*Division of Molecular Genetics, German Cancer Research Center (DKFZ), Im Neuenheimer Feld 580, D-69120 Heidelberg, Germany*

ARTICLE INFORMATION

*Article Chronology:*
Received 22 January 2007
Revised version received
4 April 2007
Accepted 5 April 2007
Available online 12 April 2007

*Keywords:*
Assembly
Keratin
Intermediate filaments
Polymorphism
Small-angle X-ray scattering
Vimentin

ABSTRACT

Intermediate filaments (IFs) represent one of the prominent cytoskeletal elements of metazoan cells. Their constituent proteins are coded by a multigene family, whose members are expressed in complex patterns that are controlled by developmental programs of differentiation. Hence, IF proteins found in epidermis differ significantly from those in muscle or neuronal tissues. Due to their fibrous nature, which stems from a fairly conserved central α-helical coiled-coil rod domain, IF proteins have long resisted crystallization and thus determination of their atomic structure. Since they represent the primary structural elements that determine the shape of the nucleus and the cell more generally, a major challenge is to arrive at a more rational understanding of how their nanomechanical properties effect the stability and plasticity of cells and tissues. Here, we review recent structural results of the coiled-coil dimer, assembly intermediates and growing filaments that have been obtained by a hybrid methods approach involving a rigorous combination of X-ray crystallography, small angle X-ray scattering, cryo-electron tomography, computational analysis and molecular modeling.



## Contents



☆ This paper is dedicated to the memory of Peter M. Steinert.

* *Corresponding author.*
E-mail address: h.herrmann@dkfz.de (H. Herrmann).

*Abbreviations:* EM, electron microscopy; IF, intermediate filament; MPL, mass-per-length; SAXS, small-angle X-ray scattering; STEM, scanning transmission EM; ULF, unit-length filament

[1] Both authors contributed equally.

0014-4827/$ – see front matter © 2007 Elsevier Inc. All rights reserved.
doi:10.1016/j.yexcr.2007.04.009

## Introduction

Initially, the term intermediate filament (IF) was coined to name a class of filaments, discovered by electron microscopy in skeletal muscle cells cultured from chick embryos, that were intermediate in diameter between actin and myosin filaments [1]. IFs represent a family of closely related filamentous biopolymers that exhibit diameters in the range of 8–12 nm. The constituent molecules, irrespective of their tissue origin, contain both highly conserved and markedly divergent features. Each IF dimer, for example, contains a pair of parallel, largely α-helical chains in axial register thereby defining a common central coiled-coil rod domain. The latter comprises four coiled-coil segments, i.e. coils 1A, 1B, 2A and 2B, of absolutely conserved amino acid number connected by three linkers termed L1, L12 and L2 (Fig. 1). Therefore, when comparing different IF proteins it is convenient to designate the residues belonging to homologous coils by their number within this element, e.g. the eleventh residue of rod segment 1A is referred to as 1A-11. The rod domain is sandwiched at its N- and C-terminus by a non-α-helical head and tail domain, respectively, and both of these domains vary greatly in size and amino acid composition from one type of IF to another. While both head and tail domains are sometimes called "globular", this designation is rather misleading, since based on their amino acid sequences they are predicted to form poorly structured and rather flexible regions. Only the lamin tails have thus far been shown to contain an evolutionarily conserved *bona fide* globular tail domain featuring an immunoglobulin-type all-beta fold (Ig-fold).

In some of the IF proteins, i.e. the keratins, the two chains of a coiled coil are homologous rather than identical, and in these cases the molecules formed are obligate heterodimers. Alternatively, the two chains may be identical and thus represent a homodimer. In essence, the rod domains associate to form the core of the IF and, by doing so, exhibit part of their tails on the filament surface thereby facilitating interactions with other cellular entities. However, those portions of the tail domains that are involved in inter-dimer interactions and which mediate IF width control are more likely to be internally located [2]. A major part of the N-terminal head domain is involved in the formation of a distinct early assembly intermediate, i.e. the tetramer. Indeed, in low salt/high pH buffer headless IF proteins form dimers rather than tetramers as do full-length cytoplasmic IF proteins under these conditions [3]. It is the basic nature of the head domains that is driving the lateral assembly of the acidic rod domains into $A_{11}$-type tetramers (see Fig. 2). More specifically, even under filament assembly conditions (i.e. 25 mM Tris–HCl, pH 7.5/150 mM NaCl) headless vimentin forms only tetramers, thereby hinting at the presence of a salt-inducible binding site which was shown to reside in coil 2 [3]. Successive amino-terminal truncation of the 12 basic arginine residues within the head domain of vimentin has revealed that tetramer and filament formation are controlled by different head segments (Herrmann et al., in preparation). Evidently, some of the basic head motifs are not essential for assembly, as they can either be removed completely or replaced by other sequence elements (see, for example, Fig. 3 in [4]). Most likely, these basic head domain segments too are displayed on the filament

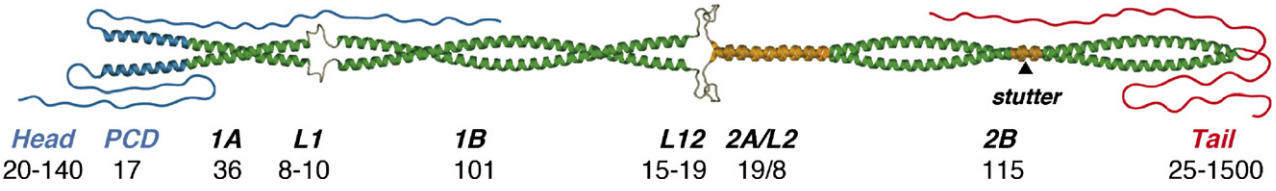


**Fig. 1 – Model of an IF coiled-coil dimer as exemplified by vimentin, a type III IF protein. The dimer is formed by a pair of parallel chains that lie in axial register in the central rod domain. Over this region the sequences of all chain types display a high degree of homology. The coiled-coil segments 1A, 1B, 2A and 2B are connected by short stretches of chain known as linkers (L1, L12, L2 respectively). In the segment 2B there is "stutter" in which a deletion of three residues occurs in what is otherwise a continuous heptad pattern. This leads to a local unwinding of the coiled-coil molecule. IF molecules may be heterodimers or homodimers depending on which chain types (I–IV) are involved. The rod domain is flanked by the "head" and "tail" domains that show wide variations in sequence between different chain types. PCD, a pre-coil domain is found in type III and type IV IF proteins. Its amino acid sequence is compatible with α-helix formation, similar to that in linker L2.**

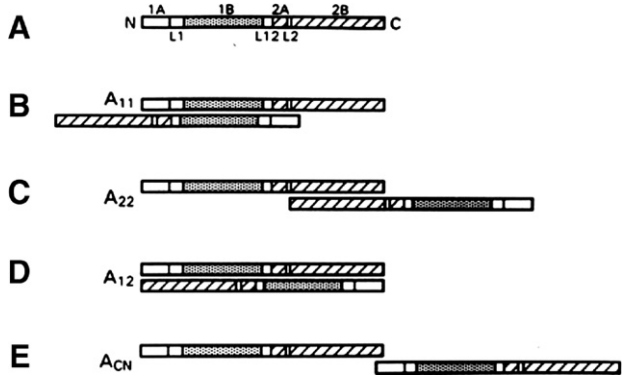


**Fig. 2 – Schematic illustration of (A) the domain structure of an individual IF dimer, (B) the $A_{11}$ mode of assembly defined by the antiparallel overlap of 1B segments, (C) the $A_{22}$ mode defined by the antiparallel overlap of 2B segments, (D) the $A_{12}$ mode defined by the antiparallel overlap of IF dimers, and (E) the parallel overlap ($A_{CN}$) between the C-terminal end of the rod domain of one dimer and the N-terminal end of the rod domain of another. It arises directly from the application of the $A_{11}$ and $A_{22}$ modes. The numerical values of the axial staggers involved in (B)–(E) are listed in Table 1 for all IF proteins except lamins. Reproduced with permission from [7].**

surface. Taken together, the observed variations in IF diameter thus relate to both the surface exposure of significant fractions of the head and tail domains, and a structural "polymorphism" exhibited by all IFs [2,5,6]. As no surprise, this polymorphism in terms of a variable number of subunits per IF cross-section has been an anathema to most structural biologists [7]. In contrast to actin filaments and microtubules, which are topologically "closed" structures and thus only allow subunit exchange at their ends, IFs are topologically "open" assemblies enabling them to exchange subunits or oligomers all along their length. It is this "subunit exchange from the side" which renders IFs polymorphic in a first instance, and most importantly, makes them highly dynamic polymers in terms of their spatial and temporal assembly, disassembly and turnover.

IFs are constructed by distinct axial and lateral arrangements of the constituent dimer building blocks, details of which have been determined by X-ray diffraction (i.e. trichocyte keratin) and intermolecular crosslinking (i.e. trichocyte keratin, epidermal keratin, vimentin, α-internexin and various co-polymers). In fact, four unique IF structures have been characterized to date: (a) epidermal and "reduced" trichocyte keratin; (b) "oxidized" trichocyte keratin; (c) the group of filaments typified by vimentin, desmin as well as the neurofilament triplet proteins; and (d) the nuclear lamins. Four distinct modes of axial alignment of dimers (known as $A_{11}$, $A_{22}$, $A_{12}$ and $A_{CN}$; see Fig. 2) have been determined experimentally for each of these, and these exhibit small but significant differences characteristic of each structure ([8–13], Table 1).

Based on in vitro assembly, filament formation occurs via a common mechanism for all vertebrate cytoplasmic IF proteins. By contrast, cytoplasmic invertebrate IF proteins and nuclear lamins exhibit alternative assembly pathways that will not be covered here [14]. Firstly, a very rapid lateral

**Table 1 – Parameters defining the molecular characteristics and modes of molecular aggregation in intermediate filaments**

| | K1/5/10/14 | Reduced α-keratin | Oxidized α-keratin | Vimentin | α-Internexin | Type III, Type IV and Type III/IV Copolymers |
|---|---|---|---|---|---|---|
| | No linkers fixed | L1, L12 and L2 Fixed | | No linkers fixed | No linkers fixed | No linkers fixed |
| $z_a$ | 79.74 | 78.15 | 50.00 | 23.89 | – | 25.06 |
| $z_b$ | 110.71 | 112.18 | 133.30 | 139.53 | 137.00 | 136.43 |
| Repeat | 301.16 | 302.51 | 316.61 | 302.95 | – | 297.93 |
| Overlap | 7.03 | 5.67 | −8.43 | 4.31 | 10.00 | 6.99 |
| $A_{12}$ | −0.70 | 3.30 | 6.98 | 5.50 | 7.00 | 4.19 |
| $A_{11}$ | −111.41 | −108.88 | −126.32 | −134.03 | −130.00 | −132.24 |
| $A_{22}$ | 189.75 | 193.63 | 190.28 | 168.92 | – | 165.68 |
| L1 | 14.84 | 14.84 | 14.84 | 11.47 | 14.50 | 10.99 |
| L12 | 12.57 | 12.57 | 12.57 | 11.99 | – | 8.99 |
| L2 | 4.77 | 4.77 | 4.77 | 7.79 | 9.00 | 8.94 |
| Δz(1BU,1BD) | −3.91 | −1.38 | −18.82 | −20.72 | – | −20.30 |
| Δz(2BU,2BD) | 2.56 | 6.45 | 3.10 | −17.34 | −19.00 | −18.24 |
| Δz(1BU, 2D) | −50.54 | −46.54 | −42.86 | −40.97 | −42.50 | −41.80 |

The parameters listed here have been refined from a least squares analysis using experimentally observed crosslink data [8–13]. The values are all expressed in multiples of $h_{cc}$, the unit rise per residue in a coiled-coil conformation (0.1485 nm). The repeat length is the molecular length minus the head-to-tail overlap that occurs between similarly directed molecules. In those situations where the overlap is negative a head-to-tail gap exists (as in oxidized trichocyte keratin). L1, L12 and L2 are the axially projected lengths of the linkers that connect coiled-coil segments 1A to 1B, 1B to 2A, and 2A to 2B respectively. $z_a$ and $z_b$ represent the axial projections of the a and b sides of the IF surface lattice structure and correspond to the axial distance between successive lattice points and between adjacent protofilaments respectively [7]. $A_{12}$, $A_{11}$ and $A_{22}$ are the axial staggers respectively between antiparallel pairs of molecules that display (i) almost complete molecular overlap, (ii) almost total overlap of the 1B segments and (iii) almost total overlap of the 2B segments. Δz(1BU,1BD), Δz(2BU,2BD) and Δz(1BU, 2D) are the axial staggers between antiparallel 1B segments, between antiparallel 2 segments (2A+L2+2B), and between antiparallel 1B and 2 segments. In one case the linkers for trichocyte keratin have been fixed at those values derived from the more numerous data obtained for the epidermal keratins.

aggregation of tetramers, each comprising two approximately half-staggered antiparallel IF dimers in the $A_{11}$ orientation, leads to the formation of about 55 nm long filaments. The number of polypeptides comprising these "unit-length" filaments has been deduced from mass measurements performed by scanning transmission electron microscopy (STEM) and ranges from 16 to 48 copies for the various types of IFs [15]. Secondly, an elongation step follows which most likely involves a complex reorganization of the dimer building blocks within the ULFs, before these anneal longitudinally to form immature IFs about 16 nm wide and several μm long. Thirdly, a radial compaction step occurs during which the molecular strands pack together more closely to eventually yield "mature" IFs [16,17]. This 3-step sequence of assembly is evidently followed by both authentic and recombinant IFs as demonstrated for desmin [15] and keratins [5,15]. Interestingly, desmin and vimentin IFs contain significantly more polypeptides per filament cross-section than keratin filaments. More specifically, type III desmin and vimentin IFs yield average mass-per-length (MPL) values of 38 and 56 kDa / nm, respectively, equivalent to 32 and 48 polypeptide chains per filament cross-section. In contrast, keratin filaments from four different sources, i.e. cultured epidermal cells, foot callus, and the living layers and stratum corneum from normal epidermis, revealed major peak values ranging from 17.0 to 20.5 and from 26.2 to 29. 5 kDa/nm (Fig. 3; see also [5]). These MPLs translate into subunits per filament cross-sections of 13 to 18 (average about 16) and 21 to 25 (average 24). On occasion, a third component was present with MPL peak values of around 36 kDa/nm, which corresponds to 32 polypeptides per filament cross-section. Taken together, these data indicate that *in vitro* reconstituted IFs are comprised of a variable number of discrete fibrillar substructures, termed protofibrils, each containing eight polypeptides per cross-section. Most likely, a very similar polymorphic sub-filamentous architecture is also encountered in IFs *in situ*. Hence, the generality of a "consensus" number of 32 subunits per IF cross-section remains elusive (Figs. 3 and 4).

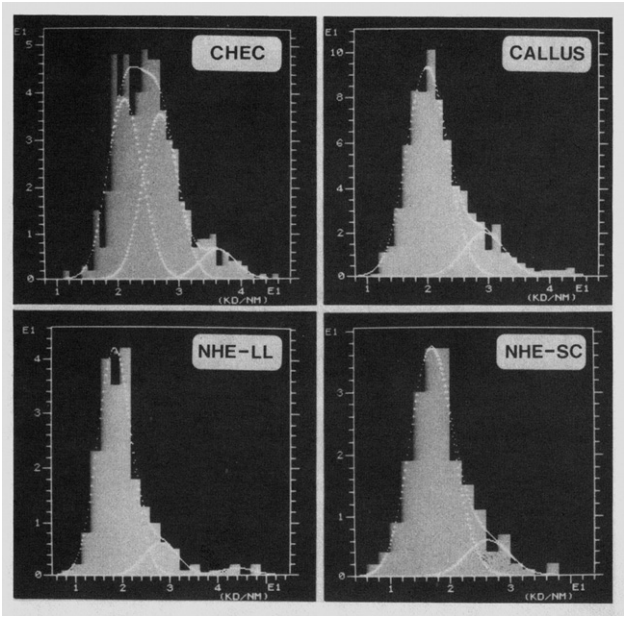


**Fig. 3 – STEM mass measurements of four different types of in vitro reconstituted human epidermal keratin filaments: CHEC, cultured epidermal cells; CALLUS, foot callus; NHE-LL, normal epidermis-stratum corneum; NHE-SC, normal epidermis-stratum corneum. Histograms of the calculated MPL values were fitted by sets of Gaussian curves. The ordinate indicates the number of segments measured, the abscissa the MPL in kDa/nm. Reproduced with permission from [5].**

## Structural analysis of the coiled-coil rod domain

### *Rod Segment 1A*

There is now a wealth of data indicating that rod segment 1A is "unusual" relative to the other two major coiled-coil rod segments (1B and 2B). The main points can be summarized as follows: (1) the coiled coil formed by the wild-type human vimentin 1A segment is only marginally stable (Burkhard et al., in preparation). Moreover, the crystal structure of a peptide representing the vimentin rod segment 1A exhibits the presence of single α-helices that are super-twisted in the same manner as seen in the GCN4 "leucine zipper" [18]. (2) Whereas the presence of a "trigger site" responsible for the initiation of coiled-coil formation has been suggested for both rod segments 1B and 2B [19], no such site has been identified in rod segment 1A based on the published trigger consensus site [20]. (3) Rod segment 1A does not display any regularity in the linear disposition of its acidic and basic residues. This is markedly different from rod segments 1B and 2B where well-defined residue periodicities are readily depicted (9.51 and 9.87 respectively). The charged-residue periodicity is likely to contribute to the definition of the molecular aggregation modes by the maximization of intermolecular ionic interactions. (4) In contrast to rod segments 1B and 2B there are few if any inter-chain ionic interactions in rod segment 1A to stabilize and specify the parallel, in-register 2-stranded coiled-coil conformation. Moreover, the vimentin rod segment 1A is monomeric in solution when the N- and C-terminal charges of the peptide chain are not neutralized by acetylation and amidation, respectively [21]. (5) In trichocyte keratin, all of the coiled-coil rod segments except 1A are involved in intermolecular disulphide bonds with other rod segments. In the case of rod segment 1A the disulphide bonds are with the head domain of the Type II chain [22].

These data have suggested a unique and dynamic role for rod segment 1A [23,24]. The model as proposed considers that rod segment 1A will form a regular two-stranded coiled-coil in the coiled-coil dimer. In addition, ionic interactions mediated by the basic head domain may stabilize this conformation. Recent X-ray crystallographic data has shown that a variant of the human vimentin rod segment 1A, in which tyrosine 16 (a core *d* position in the heptad substructure) was mutated to leucine, folds into a bona fide two-stranded coiled-coil structure (Burkhard et al., in preparation). This is in contrast to what is seen with the wild-type rod segment 1A as described above [18]. Based on this latter atomic structure of a super-twisted single α-helix,

Smith and coworkers [25] suggested a model in which two individual α-helical coil 1A segments were put together computationally to yield a 2-stranded coiled-coil rope. This model is fully compatible with the new crystal structure. In this context, the possibility of rod segment 1A being able to switch between a "2-stranded coiled-coil" and a "2-separate-α-helical-strands" conformation remains an attractive scenario in order to rationalize the highly dynamic nature of IFs and their assembly intermediates [21,23]. Most likely, the switch is set by the N-terminal head position and/or conformation, which in turn is mediated by the ionic conditions of the assembly buffer.

### *Rod Segment 1B*

This rod segment forms an α-helix with abundant aliphatic residues in *a* and *d* positions of the heptad pattern. Hence, two helices should generate a stable coiled coil. Indeed, as demonstrated by analytical ultracentrifugation coil 1 is dimeric in solution, and therefore one has to conclude that the rod 1B segment mediates coiled-coil formation, since the rod 1A segment is supposed to form a weak coiled coil only (see above and [21]). Nevertheless, several interesting structural features have not been solved yet. First, what is the exact start of the coil? Taking vimentin as a paradigm, both glycine 147 and tyrosine 150 are potential start sites [21]. With respect to the end of the coiled coil, it seems that leucine 245 is the last amino acid in a rather continuous heptad pattern, although the α-helix may continue. Notably, the following amino acids are highly conserved in cytoplasmic IF proteins. In type I to IV proteins the sequence reads: QAQIQ. Only immediately preceding the initiation of rod segment 2A, we find a proline in vimentin, the small neurofilament protein (NFL) and keratin 18 [17]. Moreover, since there are at the end of rod segment 1B many charged amino acids in *b*, *c*, *e*, *f* and *g* positions as well as the last *d* position, i.e. coil 1B residue 116 is a glutamic acid in practically all IF proteins, future structural studies will have to reveal the true structure of this "transitional" domain between rod segment 1B and linker L12.

In this context, it is worth noting that coil 1B of invertebrate cytoplasmic IF proteins and the nuclear lamins harbors a 42-amino-acid insertion relative to the vertebrate cytoplasmic IF proteins. It is generally assumed that these 6 heptads were lost as one contiguous piece during evolution, however, another sequence alignment is also possible that considers the independent loss of two and four heptads at different coil 1B positions, respectively [17]. Yet another interesting structural feature exhibited by the nuclear lamins is the linker L12. It differs significantly from that of the cytoplasmic IF proteins, and it has been suggested to form an α-helical fold [26]. Whatever the case, this "linker" provides limited flexibility only. Notably, lamin dimers appear rather straight in electron micrographs obtained by glycerol spraying/rotary metal shadowing (see, e.g. [27–29]). Notably, also the head-to-tail associations formed from these dimers are remarkably linear with little bending, quite different from what would be expected if a flexible linker was present. Again, we have to await the crystal structure determination of these domains for a more rational explanation.

### *Rod Segment 2A and Linker L2*

Segment 2A, the shortest (19 residues) of the four α-helical rod domain segments in IF molecules, contains a classical heptad substructure with apolar residues that are alternately three and four residues apart (average apolar separation 3.5 residues). Since the average number of residues per turn in a "standard" α-helix is greater than 3.5 (i.e. about 3.63), these residues generate an hydrophobic stripe on the surface of each monomer α-helix that winds around its axis in a left-handed manner. This is consistent with chain aggregation and the adoption of a left-handed coiled-coil conformation that shields the apolar residues from the polar environment. Very recently, however, Parry [30] observed that the sequences of rod segment 2A and linker L2 also contained an underlying 11-residue-repeat substructure, a feature again characterized by the disposition of apolar residues. In this case the average separation of clumps of apolar residues is 3.67 residues (i.e. 11/3). The implication of this observation is that the hydrophobic stripe on the surface of the α-helices becomes nearly parallel to its axis and therefore the two-stranded left-handed coiled-coil structure is essentially transformed into a parallel α-helical bundle. X-ray crystallographic data on the 11-residue-repeat coiled-coil structures of tetrabrachion [31,32] and RH4 [33] support this prediction. Several provisos, however, must be noted here. Firstly, a degenerate, double 11-residue repeat in apolipoproteins does lead to a left-handed rather than a right-handed coiled coil. Secondly, the number of consecutive 11-residue repeats (2.5) in IF proteins is less than that seen in proteins with an experimentally-derived 11-residue-repeat structure. Thirdly, some apolar positions in an 11-residue repeat are more inclined towards the core of the coiled-coil than would be the case for a heptad repeat. This imposes some physical constraint of the sizes of the apolar residues involved and, in the case of IF molecules, the generally large apolar residues could induce significant distortion. Crystallographic data on rod segment 2A and linker L2 are thus required to resolve this conformational dilemma in an unequivocal manner.

An alternative approach to X-ray crystallography to obtain conformational data has been the use of site-directed spin labeling in conjunction with electron paramagnetic resonance (SDSL-EPR). Hess and colleagues [34] have recently studied the L2 region of human vimentin by making single-cysteine substitutions covering the 24-residue region starting with residue 18 of rod segment 2A through linker L2 and up to residue 13 of rod segment 2B. In contrast to theoretical studies, the EPR results indicate that linker L2 is rigid and not flexible. In particular, residues 1 each of linker L2 and rod segment 2B that delineate the ends of linker L2 are shown to be in close proximity to their partners on adjacent strands (in fact, they are about 1 nm apart) and, furthermore, they interact more strongly than residues in internal *a* and *d* positions in a coiled coil. This, together with moderate dipolar line broadening data relating to several of the residues lying in between, suggests that a close association exists between the two strands over the entire length of linker L2. Three charged residues, i.e. residues 4 and 6 of linker L2 and residue 4 of rod segment 2B (that are all largely but not absolutely conserved in type I–III IF protein chains) have also been

implicated as involved in stabilizing interchain ionic interactions. This implies that linker L2 may represent a special site at which the antiparallel alignment of dimers is facilitated or, alternatively, is one with importance in initiating dimer formation. However, no spectra characteristic of a left-handed coiled-coil conformation have been recorded for linker L2. However, it should be considered that both the introduction of a cysteine as well as its conjugation with a bulky EPR probe could introduce significant alterations into the protein thereby influencing protein–protein subunit interactions tremendously. We found that corresponding modifications in vimentin with biotin coupled to cysteines led to a complete decay of its assembly properties (data not shown). In line with this, even minor changes of the amino acid character as introduced by disease mutations in desmin can drastically alter the assembly properties of this protein in an entirely unpredictable manner [35].

### *Rod Segment 2B*

In addition to the EPR evidence that the left-handed coiled coil in rod segment 2B becomes recognizable at residue 12 (2B-12) there is X-ray crystallographic data for the structure of the C-terminal region of human vimentin (residues 40 to 115 of rod segment 2B, i.e. a major part of the 2B rod segment [18,36] and human lamins A/C and B (residues 39 to 121 of rod segment 2B [37]). Two features of particular importance relate (i) to the C-terminal of segment 2B (7–10 residues) in which the chains splay apart and deviate significantly from the coiled-coil geometry seen in the remaining part of the structure, and (ii) to the highly conserved stutter region (close to and around residue 59 of rod segment 2B) in which the two chains unwind and give rise to a much longer coiled-coil pitch length over a localized region [38,39]. The observation that the molecules have a head-to-tail overlap in the filament (determined from intermolecular crosslinking data) allied to the fact that the C-terminal end of rod segment 2B splays suggests that the molecules interdigitate and form a four-stranded α-helical bundle with all four strands similarly directed [25,37]. A complex of the overlap region has not yet been crystallized, however. Modeling shows that charged groups in the head and tail domains are likely to be involved in stabilizing this polar head-to-tail interaction [37].

## Human keratin chain analyses: promiscuous heterodimers

The human genome project has allowed the sequences of all hair and epithelial keratin intermediate filament proteins to be determined (11 type I and six type II IF chains in hair keratin, and 17 type I and 20 type II IF chains in epithelial keratins). This provided a substantial database on which to base a significant study of the features of structural and functional interest in IF molecules whose origins lie in their constituent sequences [40]. The results can be briefly summarized as follows:

(a) The common acidic and basic residue periodicity in segment 1B (9.51±0.14 residues) is significantly different from that seen in the equivalent groups in segment 2B (9.87±0.15 residues), thereby implying a preference for the $A_{11}$ and the $A_{22}$ mode over the $A_{12}$ mode of molecular aggregation. Equally as important as this difference is the fact that the probability of the former occurring by chance is statistically much lower than it is for the latter. This implies that the period in segment 1B is more regular than it is in segment 2B and gives a hint towards explaining the experimental fact that the $A_{11}$ rather than the $A_{22}$ mode represents the initial step in the assembly process of vimentin [3]. Also, the observation that the phasing of the acidic residues differs from that of the basic residues by about 160–165° (and not 180°) agrees well with the experimentally observed antiparallel alignment of dimers rather than a parallel one, a view confirmed from crosslink data.

(b) Rod domain segment flexibility data show that segment 2A is the least flexible in both chain types and in both hair and epithelial keratins, and that linker L1 is among the most flexible regions. The latter is important with regard to the special role played by segment 1A and what may prove to be an "unusual" coiled-coil conformation adopted by segment 2A.

(c) The higher percentage α-helix contents of the (major) coiled-coil segments 1B and 2B in type II chains relative to those in type I chains when each is in a monomeric form in solution suggests that the type II chains may act as a template for dimer formation.

(d) Inter-chain ionic interactions invariably specify a parallel in-register chain arrangement in the IF molecule but do not distinguish clearly between various chain combinations, thereby indicating the important role of other residues (probably those in *a* and *d* positions that are located along the interface between the two chains that together form the dimer) in specifying the chain combinations that occur in the IF molecules in vivo.

(e) The unequal numbers of IF type I and type II chains indicate the formation of promiscuous heterodimers, i.e. more than one type I chain may be able to interact with the same type II chain (and vice versa) to form a heterodimer.

(f) The occasional presence (temporally) of a single chain type suggests the possibility of transient populations of homodimers.

(g) The necessity of a heterodimer structure for keratins but not for others such as type III vimentin homodimers indicates that some IF molecules require greater structural and functional specificity than others. Two possible reasons have been advanced. The first relates to what appears to be a very considerable number of other molecules that both hair and epithelial keratins are known to interact with. It can thus be argued that this requires a greater number of specific sites of interaction especially with regard to the head and tail domains that show the greatest differences between chain types. A heterodimer is necessarily better suited to meet this demand than is a homodimer. A second reason relates to the observation that hair keratin has two distinct structures, one relating to that formed at the base of the follicle in a reducing environment and

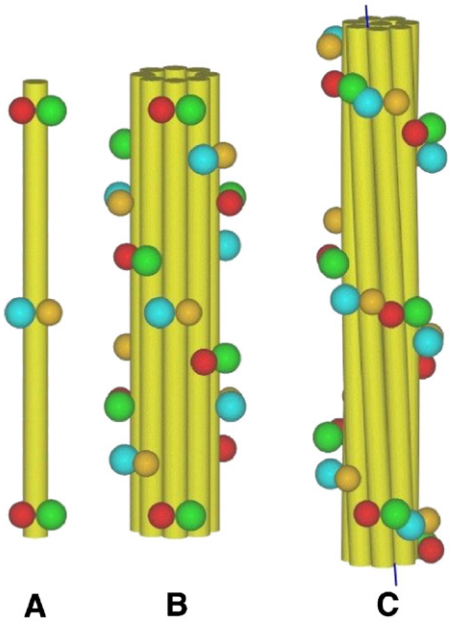


**Fig. 4 – Generic models for the three-dimensional structure of reduced and oxidized trichocyte IF. The IF can be regarded as composed of eight protofilaments each, i.e. tetramers, consisting of a pair of oppositely directed molecular strands, i.e. dimers. (A) A single protofilament in the reduced IF. The yellow cylinders represent the helical domains of the constituent molecules, the green spheres represent the N-terminal domains of the Up molecular strands and the blue spheres to those of the Down molecular strands. The red spheres represent the C-terminal domains in the Up molecular strands and the orange spheres represent the C-terminal domains of the Down molecular strands. The axial period is 44.92 nm. The radial disposition of the segments in the helical domain is currently unknown and is represented here diagramatically. Since there is an overlap between segments 2B and 1A the protofilament will be three molecular strands in width over short lengths. (B) The reduced IF is visualized as containing eight protofilaments arranged regularly on a ring of radius 3.5 nm. Each protofilament is related to its predecessor by a rotation of 45° and an axial displacement of 16.85 nm. The end groups fall on a two-start left-hand helix that, at low resolution, would appear as diagonal banding pattern with a spacing of 22 nm. (C) The (7+1) arrangement for oxidized IF in hydrated keratin is based on one of the two possible surface lattice structures derived from X-ray diffraction studies that are also compatible with other data. It differs from that of the (8+0) model for reduced keratin IF in several respects. Firstly, seven protofilaments are assembled on a ring of radius 3.0 nm, each related to its predecessor by a rotation of 30.7° and an axial displacement of 19.82 nm. These surround a central, straight protofilament. Secondly, it follows that the surface lattice structure is different from that in the reduced model but the axial period in an individual protofilament remains unchanged at 47.0 nm. Thirdly, the end domains are now in much closer proximity than in the reduced model and give the appearance of being distributed on a helix of pitch 23.5 nm.**

another that occurs when the conditions become oxidizing at the time of cell death (Fig. 4). The latter results in a highly stable disulphide-bonded structure. Although not yet characterized in any detail, a similar – probably identical – two-state structure may be present in cells in epithelial tissues. Any requirement for a structural transition of this magnitude would require considerable specificity if it was to occur efficiently. Once again, a heterodimer structure would seem better suited to do this than would a homodimer.

## Small angle X-ray scattering studies of vimentin intermediates

As noted earlier there are very few structural details available of the intermediates involved in IF formation, whether they be tetramers, octamers or ULFs. To address this issue, small-angle X-ray scattering (SAXS) has been employed recently [41]. This approach is based on analyzing the IF protein of interest in solution, whereas the buffer composition as well as the salt concentration can be adjusted to induce gradual assembly in a controlled fashion. Along these lines, a successful screening was undertaken for human vimentin solutions to find conditions that give rise to specific oligomeric species, thus allowing each of them to be characterized structurally. The SAXS signal carries information about the shape of the solute molecule at the nanometer scale. It has to be noted that the information obtainable using SAXS is less detailed than that gained using X-ray crystallography, and does not quite reach atomic resolution. Nonetheless, using the available three-dimensional structural model of the elementary dimer as a starting point as well as additional experimental knowledge such as the chemical cross-linking data, it was possible to build atomic models of assembly intermediates that were well compatible with the observed SAXS data. More precisely, good agreement could be obtained between the model-calculated and the experimental SAXS curves. As the result, a number of interesting conclusions have been drawn:

(a) In 10 mM Tris–HCl buffer (pH 8.4), the tetrameric species was predominant. The model for the tetramer used as a starting point an antiparallel, half-staggered arrangement of two dimers corresponding to the $A_{11}$ mode, following a considerable body of crosslinking and biochemical evidence (Fig. 5A). The refinement of the relative position of the two dimers against the collected SAXS data upon considering each dimer as a rigid body placed the axes of the dimers parallel to one another and 3.4 nm apart (Fig. 5B). This means that the two coiled coils are separated too much for a direct interaction and most likely need to be held together by the positively charged head domains.
(b) Upon the gradual addition of NaCl up to 20 mM while keeping the pH constant at 8.4, the formation of the octameric species became apparent both from the SAXS data and analytical ultracentrifugation. The octamer model (Figs. 5C, D) was based on a pair of the previously refined tetramers. The tetramers were linked to one

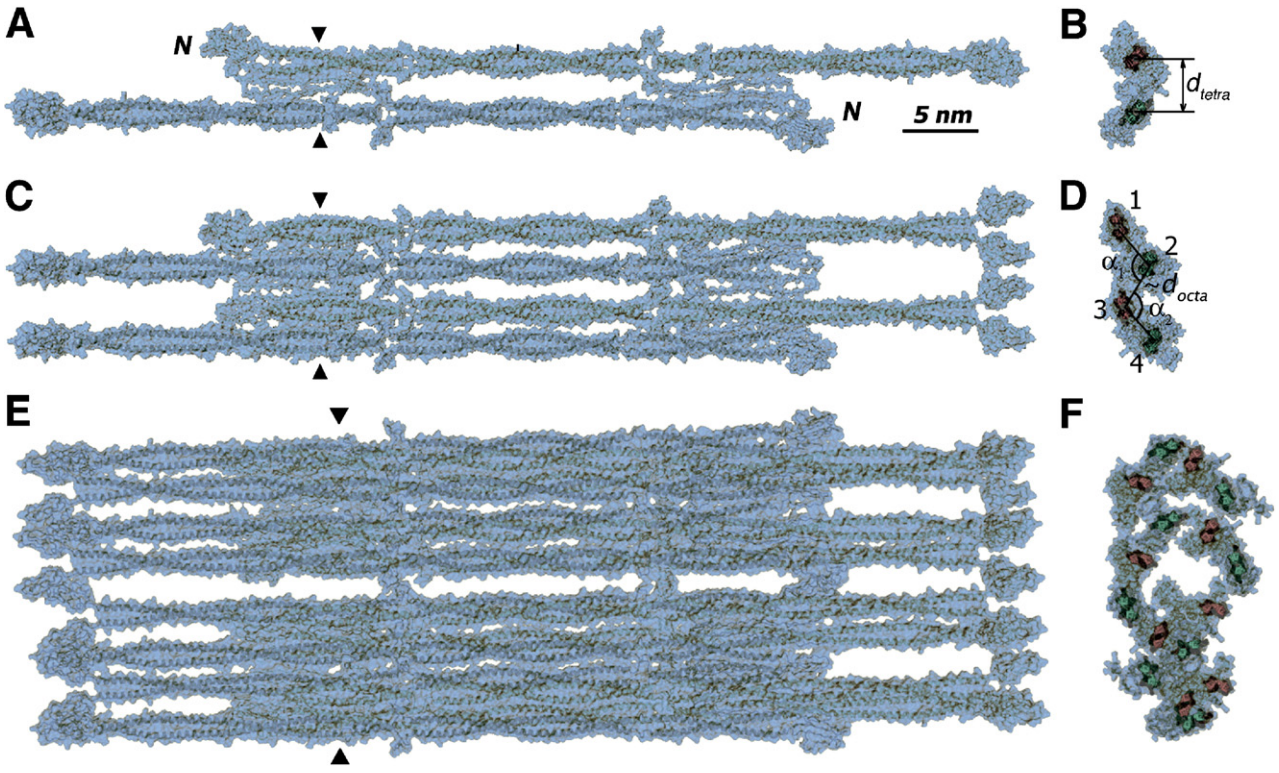


**Fig. 5 – Atomic models of vimentin tetramer (A, B), octamer (C, D) and the unit-length filament comprising four octamers (E, F) as derived from SAXS data [41]. For each model, two orthogonal views are shown.**

another with a further $A_{11}$ mode of molecular aggregation, this time between one dimer in each of the two tetramers. A chair-like conformation of the four dimers, however, was required to fit the SAXS data, and the angle of puckering was determined to be 107°. The dimer axes were parallel in the final refined structure and their separation was ~3.2 nm. The cross-section of the refined tetramer fits within an ellipse with a major axis of 10.5 and a minor axis of 5.0 nm.

(c) The unit-length filament (ULF) species were predominant in 10 mM Tris–HCl buffer (pH 8.4) with 75 mM NaCl. The ULF model was constructed from four refined octamers, each of which is related to the next one by $A_{11}$ contacts between connecting dimers (Figs. 5E, F). For a structure with strict four-fold symmetry, the cross-section was not only too large but had an inappropriate shape to fit the SAXS data, which instead suggested an oval cross-section. The final refined ULF model has average dimensions of 9 nm × 16 nm × 65 nm. Importantly, the mass is distributed fairly evenly over the cross-section of the ULF, with only a minor void situated in its very middle. At the same time, SAXS data clearly suggest that the dimers within the ULF are relatively loosely packed, and there are plenty of possibilities for further rearrangements during the compaction of the elongated filament.

While these in vitro studies necessarily used buffer and ionic strength that favored a specific assembly intermediate, they nevertheless represent an important first step towards the understanding of how the lateral assembly of sub-IF units may occur in vivo, starting with the soluble tetramers that appear to be present in the cytoplasm. Ideally, much higher resolution X-ray diffraction studies will be necessary to gain more detailed structural insight, but the difficulty of obtaining crystals of such assemblies is indeed very high (Fig. 6).

## IF assembly

An extraordinary example of an IF that changes its structure both axially and laterally is provided by trichocyte keratin. Synthesis and assembly of hair keratin IF molecules occur in a reducing environment in the column of cortical cells immediately above the dermal papilla. IF-associated proteins (IFAP) are deposited between and interdigitate with the IF at a later stage towards the end of IF synthesis. Further up the hair follicle during terminal differentiation and cell death the cellular environment changes to an oxidizing one and disulphide bond formation takes place. Two significant structural effects are observed. Firstly, molecular slippage occurs within the protofilaments (these are four chains in section and structurally “equivalent” to half a protofibril) and this is characterized by a change in $A_{11}$ from −16.65 nm to about −19.3 nm (values are either −19.18 and −19.42 nm depending on whether or not certain parameters are constrained in the refinement procedures employed with the crosslinking data, see Table 1). This event, it has been postulated, is precipitated by interactions between the terminal domains of the IF molecules.

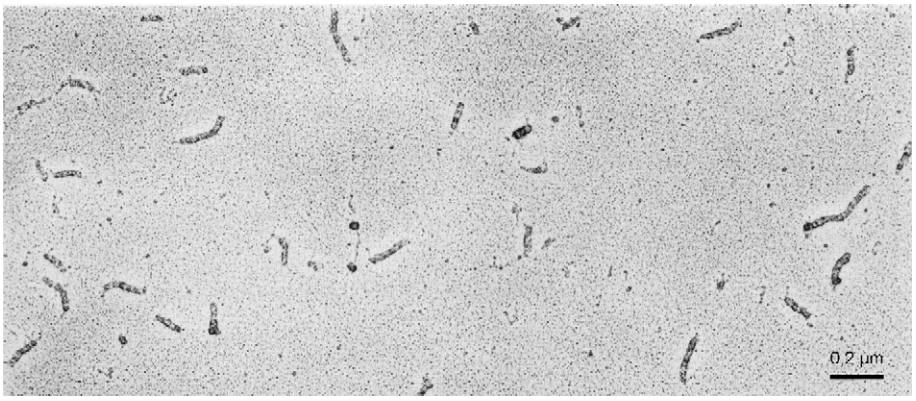


**Fig. 6 – Electron micrograph of glycerol-sprayed/ rotary metal shadowed preparations from solubilized denatured bovine snout epidermis keratin on dialysis against 1 mM Tris–HCl, pH 8.0, for 12 h. Bar, 200 nm. Reproduced with permission from [46].**

In addition to this axial re-arrangement, the lateral dimensions of the IF change upon oxidation. Er Rafik and colleagues have used X-ray microdiffraction to study the hair follicle at a variety of histology-based growth zones [42]. Their conclusions are that in the immediate vicinity of the bulb IFs have a low-density core and a diameter of about 10 nm. Further up the follicle the IF diameter was seen to be smaller and was estimated to be about 7.5 nm. Fraser and Parry have subsequently shown that the data from Er Rafik and coworkers [42] can be best explained by a ring of electron density with a radius of about 3.5 nm [43]. In the fully keratinized (oxidized) hair the same ring of electron density on which the protofilaments are situated has a radius of about 3.0 nm [42,44,45]. These datasets are physically compatible with the equivalent of eight protofilaments forming the ring in the reduced form and seven (with one central) in the oxidized case. In both instances the data are compatible with surface lattices that are both continuous and perfect [43]. Hence, in this case we do not encounter a four-protofibrillar substructure (Fig. 4).

IFs naturally segregate into three assembly groups, i.e. lamins, keratins and vimentin-like proteins, and similar types of assembly intermediates have been found at least for the latter two members. For this assembly scenario, the ULF concept has allowed us to take a decisive deeper insight in the mechanism of filament formation [16], in particular in the context of a group of desmin disease mutants that were demonstrated to cause the termination of the assembly process at different distinct stages of assembly corresponding to those postulated by the ULF model [35]. ULFs have been observed before several times, but they were not initially recognized as principal assembly nuclei and elongation units of filament formation. In an early study it was demonstrated that purified epidermal keratins from bovine muzzle would form various intermediates when reconstituted from 8 M urea into buffers that did not favor IF assembly. Therefore, the electron microscope analysis of such intermediate stages of "incomplete" filament assembly revealed – in addition to protofibrillar and ringlet-type structures as well as "tuftlike bundles of loosely fasciated protofilaments" [46] – "more compact" and stiff filaments of 40 to 400 nm length (Fig. 6). These structures look very much the same like those identified for simple epithelial keratins, K8 and K18, by a "time lapse"-type kinetic EM regime [47]. Furthermore, ULF-like structures of vimentin were observed by the group of Richard Robson [48,49]. They employed conditions that impede the formation of IFs, i.e. buffers of high pH (8.5) with 20 to 50 mM NaCl, and were able to document the formation of 50 nm long full width filaments by quick freeze, deep-etch methods. However, it was not considered that these "ULFs" were the direct units for further elongation to form mature IFs and not tetramers. Interestingly, it was observed that occasional breaks were present along some filaments "suggesting that annealing between short IF is possible" [49]. Last but not least, ULFs were reported for neuronal proteins such as α-internexin to be the prominent first assembly products [50]. Interestingly, STEM mass measurements determining the mass-per-length values for vimentin, desmin and neurofilament protein L (NFL) revealed that at the ULF stage the characteristic numbers of molecules per cross-section are identical to those finally determined for the mature IFs [51].

## Cryo-electron tomography of IFs

The 3-D molecular architecture of microtubules and microfilaments is well established at intermediate and near-atomic resolution, whereas for IFs these data are missing. However, very recent results demonstrated that with IFs cryo-electron tomography also promises to reveal essential structural details of the filament ([52] and the article by Norlen and colleagues, this issue). Hence, with this method it is obvious that within the mature vimentin filament a protofibrillar-type arrangement of subunits exists exhibiting in cross-section four to five strands arranged in a circular fashion. Both the microscopy with mature vimentin filaments and SAXS data of ULFs suggest that in cross-section the octameric strands form a cylinder with a small void along the filament axis rather than with a central core like in the model proposed for oxidized keratins (Fig. 4C).

Such an organization of the filament has already been observed in the beginning of IF research by electron microscopy of ultrathin sections prepared from cultured cells. Werner Franke and colleagues used colcemid to induce

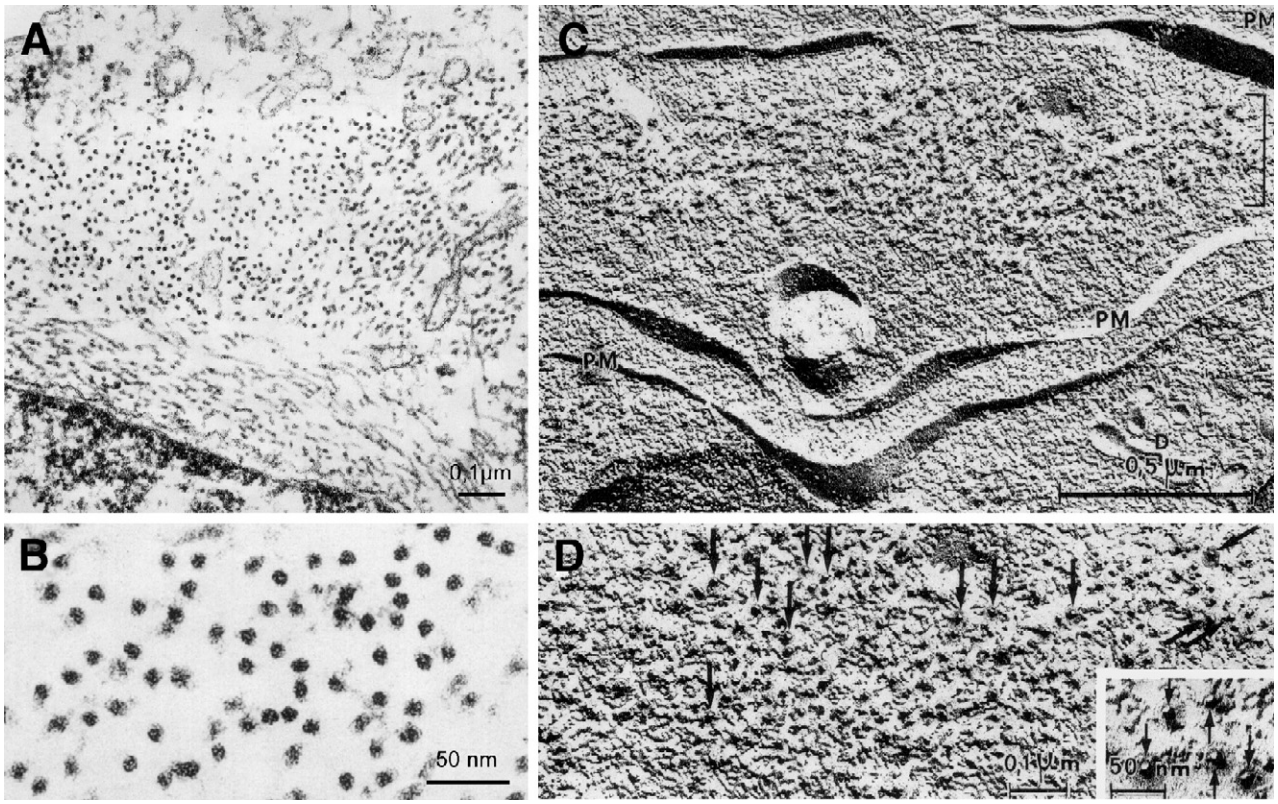


**Fig. 7 – Electron microscopic analysis of perinuclear bundle aggregates of vimentin filaments obtained with colcemid treated vascular smooth muscle derived rat cells (RVF-SMC). (A) Thin section revealing many filaments are arranged in parallel. N, nucleus. Bar, 100 nm. (B) Enlarged detail from within the vimentin bundle. (C, D) The appearance of a vimentin filament bundle in freeze-etch preparations of RVF-SM cells treated with colcemid. The bracket in (C) denotes the margins of a bundle cross-fracture. PM, plasma membrane; D, dictyosomes. The arrows in (D) and the inset indicate ringlet structures demarcated at one side by a metal shadow deposit. Reproduced with permission from [53].**

the formation of perinuclear bundles of vimentin IFs in rat vascular smooth muscle-derived cells (RVF-SMC) and visualized their outline both by conventional thin section TEM as well as by freeze-fracture techniques [53]. With both techniques it is clear that IFs in cells have a cylindrical structure (Fig. 7). In particular, the freeze fracture images indicate that IFs may have a small but visible central hollow core (arrows in Figs. 7C and D).

## Future directions

Future developments regarding IF structure are likely to come from the application of both current techniques and newer ones that are now beginning to appear. In the former category it is to be expected that X-ray crystallography applied to well-defined IF fragments, small-angle X-ray scattering (SAXS) applied to sub-IF assemblies and X-ray microdiffraction applied to intact specimens, will all continue to prove their worth as will the use of site-directed spin-labeling allied to electron paramagnetic resonance and AFM to probe IF nanomechanics. In particular, there has been a significant improvement of the SAXS technique in the last few years, as regards both the quality of the experimental data arising from the use of highly brilliant synchrotron X-ray sources and the efficiency of newest data processing algorithms [54,55].

Mutations of various IF chains are also beginning to throw some light on key aspects of structure, although it is generally true that an explanation of how a particular mutation leads to the effect observed in a diseased tissue is proving elusive. Initial attempts in this direction involved three-dimensional computer modeling (see, for example, Smith et al. in their molecular dynamics study of 22 epidermolysis bullosa simplex (EBS) mutations in segment 1A of K5/K14 cytokeratin intermediate filaments [56], or Kaminska et al. [57] and Pruszczyk et al. [58] for molecular modeling of desminopathy mutations). However, definite insights on the mechanism of various disease-related mutations will have to await experimental proof. Moreover, it has been demonstrated by analysis of the assembly behavior of the corresponding recombinant proteins that these mutant proteins can behave quite normally, at least in vitro and in particular in the presence of wild type desmin. This is in contrast to the predictions made from the modeling data [59]. Here, the information on the particular stage at which any given mutation starts to adversely affect the assembly pathway can be very effectively obtained by a systematic SAXS study in solution and may complement the data obtained by EM of in vitro assembled desmin mutants [35,60,61]. Moreover, the ultimate information on the precise

influence of a mutation on the atomic structure of the dimer should be obtained using X-ray crystallography on carefully designed fragments carrying such mutations.

Amongst the newer methods to emerge in the last few years is cryo-electron tomography. Conventionally, for electron microscopy chemical methods thought to preserve structure in the specimens have been used, but it is still difficult to distinguish induced artifacts from the "real" structure. Cryo-methods, on the other hand, involve hydrated, unstained specimens that are rapidly frozen (typically 20 ms duration), sometimes in combination with high pressure, to avoid ice formation. This results in specimens of greatly enhanced quality that give rise to images that may more likely reflect the genuine ultrastructure. Using cryo-electron tomography new interesting details are now beginning to emerge, to add to the already available knowledge, obtained through conventional EM as well as atomic force microscopy, on the protofibrillar substructure of IF, the handedness of the supercoiling that the protofibrils exhibit and their corresponding pitch length. It can be expected that further structural data from this source will yield important new insights into IF structure in the near future.

## Concluding comments

It has become increasingly clear that IFs endow a cell with sufficient resilience to withstand both the mechanical and non-mechanical stresses to which it is normally subject, thus preventing any compromise of cellular function. IFs may thus be said to be sensors and integrators of the cellular interior under stress. This crucial ability to a cell's well-being resides in the structure and mechanics of the IFs, a subject well worthy of the widespread attention that it has received over the past 25 years. Although much is now understood about the primary, secondary and tertiary structure of intermediate filaments proteins and sub-IF assemblies, a great deal more information will be required before a full appreciation can be gained of the structural sophistication displayed by these important cellular filaments. When such information is at hand it will, in turn, allow better insight into the various functions that the different types of IFs undertake within their specific environs in the respective cells they are expressed in.

## Acknowledgments

Harald Herrmann and Ueli Aebi wish to thank Werner W. Franke for his continuous interest in our work and for providing original reprints of papers that are unfortunately not even listed by Pubmed any more. H. H. acknowledges grants from the German Research Foundation (DFG, HE 1853/4-2 and 4-3). S.V.S. is funded in part by a grant from the Group Biomedical Sciences, Catholic University of Leuven, and from the Swiss Society for research on Muscular Diseases. The STEM work was funded by the Swiss National Foundation Grant (number SNF 501 221) to Andreas Engel (Biozentrum, Basel), whom we thank for his support. U.A. was funded by a research grant and an NCCR program grant on "Nanoscale Science" by the Swiss National Science Foundation, the Swiss Society for Research on Muscular Diseases, the M.E. Müller Foundation of Switzerland, and the Canton Basel Stadt. Last but not least, H. H. and U. A. acknowledge support from the European Union FP6 Life Science, Genomics and Biotechnology for Health area (LSHM-CT-2005-018690).

## REFERENCES

[1] H. Ishikawa, R. Bischoff, H. Holtzer, Mitosis and intermediate-sized filaments in developing skeletal muscle, J. Cell Biol. 38 (1968) 538–555.
[2] H. Herrmann, M. Häner, M. Brettel, S.A. Muller, K.N. Goldie, B. Fedtke, A. Lustig, W.W. Franke, U. Aebi, Structure and assembly properties of the intermediate filament protein vimentin: the role of its head, rod and tail domains, J. Mol. Biol. 264 (1996) 933–953.
[3] N. Mücke, T. Wedig, A. Bürer, L.N. Marekov, P.M. Steinert, J. Langowski, U. Aebi, H. Herrmann, Molecular and biophysical characterization of assembly-starter units of human vimentin, J. Mol. Biol. 340 (2004) 97–114.
[4] M. Reichenzeller, A. Burzlaff, P. Lichter, H. Herrmann, In vivo observation of a nuclear channel-like system: evidence for a distinct interchromosomal domain compartment in interphase cells, J. Struct. Biol. 129 (2000) 175–185.
[5] R. Eichner, P. Rew, A. Engel, U. Aebi, Human epidermal keratin filaments: studies on their structure and assembly, Ann. N. Y. Acad. Sci. 455 (1985) 381–402.
[6] A. Engel, R. Eichner, U. Aebi, Polymorphism of reconstituted human epidermal keratin filaments: determination of their mass-per-length and width by scanning transmission electron microscopy (STEM), J. Ultrastruct. Res. 90 (1985) 323–335.
[7] D.A. Parry, P.M. Steinert, Intermediate Filament Structure, Springer Verlag, New York/Berlin/Heidelberg, 1995.
[8] P.M. Steinert, L.N. Marekov, R.D. Fraser, D.A. Parry, Keratin intermediate filament structure. Crosslinking studies yield quantitative information on molecular dimensions and mechanism of assembly, J. Mol. Biol. 230 (1993) 436–452.
[9] P.M. Steinert, L.N. Marekov, D.A. Parry, Conservation of the structure of keratin intermediate filaments: molecular mechanism by which different keratin molecules integrate into preexisting keratin intermediate filaments during differentiation, Biochemistry 32 (1993) 10046–10056.
[10] P.M. Steinert, L.N. Marekov, D.A. Parry, Diversity of intermediate filament structure. Evidence that the alignment of coiled-coil molecules in vimentin is different from that in keratin intermediate filaments, J. Biol. Chem. 268 (1993) 24916–24925.
[11] P.M. Steinert, L.N. Marekov, D.A. Parry, Molecular parameters of type IV alpha-internexin and type IV–type III alpha-internexin-vimentin copolymer intermediate filaments, J. Biol. Chem. 274 (1999) 1657–1666.
[12] P.M. Steinert, Y.H. Chou, V. Prahlad, D.A. Parry, L.N. Marekov, K.C. Wu, S.I. Jang, R.D. Goldman, A high molecular weight intermediate filament-associated protein in BHK-21 cells is nestin, a type VI intermediate filament protein. Limited co-assembly in vitro to form heteropolymers with type III vimentin and type IV alpha-internexin, J. Biol. Chem. 274 (1999) 9881–9890.
[13] D.A. Parry, L.N. Marekov, P.M. Steinert, Subfilamentous protofibril structures in fibrous proteins: cross-linking evidence for protofibrils in intermediate filaments, J. Biol. Chem. 276 (2001) 39253–39258.

[14] N. Geisler, J. Schunemann, K. Weber, M. Häner, U. Aebi, Assembly and architecture of invertebrate cytoplasmic intermediate filaments reconcile features of vertebrate cytoplasmic and nuclear lamin-type intermediate filaments, J. Mol. Biol. 282 (1998) 601–617.
[15] H. Herrmann, M. Häner, M. Brettel, N.O. Ku, U. Aebi, Characterization of distinct early assembly units of different intermediate filament proteins, J. Mol. Biol. 286 (1999) 1403–1420.
[16] H. Herrmann, U. Aebi, Intermediate filament assembly: fibrillogenesis is driven by decisive dimer–dimer interactions, Curr. Opin. Struct. Biol. 8 (1998) 177–185.
[17] H. Herrmann, U. Aebi, Intermediate filaments: molecular structure, assembly mechanism, and integration into functionally distinct intracellular Scaffolds, Annu. Rev. Biochem. 73 (2004) 749–789.
[18] S.V. Strelkov, H. Herrmann, N. Geisler, T. Wedig, R. Zimbelmann, U. Aebi, P. Burkhard, Conserved segments 1A and 2B of the intermediate filament dimer: their atomic structures and role in filament assembly, EMBO J. 21 (2002) 1255–1266.
[19] T. Mehrani, K.C. Wu, M.I. Morasso, J.T. Bryan, L.N. Marekov, D.A. Parry, P.M. Steinert, Residues in the 1A rod domain segment and the linker L2 are required for stabilizing the A11 molecular alignment mode in keratin intermediate filaments, J. Biol. Chem. 276 (2001) 2088–2097.
[20] R.A. Kammerer, T. Schulthess, R. Landwehr, A. Lustig, J. Engel, U. Aebi, M.O. Steinmetz, An autonomous folding unit mediates the assembly of two-stranded coiled coils, Proc. Natl. Acad. Sci. U. S. A. 95 (1998) 13419–13424.
[21] S.V. Strelkov, H. Herrmann, N. Geisler, A. Lustig, S. Ivaninskii, R. Zimbelmann, P. Burkhard, U. Aebi, Divide-and-conquer crystallographic approach towards an atomic structure of intermediate filaments, J. Mol. Biol. 306 (2001) 773–781.
[22] H. Wang, D.A. Parry, L.N. Jones, W.W. Idler, L.N. Marekov, P.M. Steinert, In vitro assembly and structure of trichocyte keratin intermediate filaments: a novel role for stabilization by disulfide bonding, J. Cell Biol. 151 (2000) 1459–1468.
[23] D.A. Parry, L.N. Marekov, P.M. Steinert, T.A. Smith, A role for the 1A and L1 rod domain segments in head domain organization and function of intermediate filaments: structural analysis of trichocyte keratin, J. Struct. Biol. 137 (2002) 97–108.
[24] S.V. Strelkov, H. Herrmann, U. Aebi, Molecular architecture of intermediate filaments, BioEssays 25 (2003) 243–251.
[25] T.A. Smith, S.V. Strelkov, P. Burkhard, U. Aebi, D.A. Parry, Sequence comparisons of intermediate filament chains: evidence of a unique functional/structural role for coiled-coil segment 1A and linker L1, J. Struct. Biol. 137 (2002) 128–145.
[26] P.M. Steinert, D.R. Roop, Molecular and cellular biology of intermediate filaments, Annu. Rev. Biochem. 57 (1988) 593–625.
[27] U. Aebi, J. Cohn, L. Buhle, L. Gerace, The nuclear lamina is a meshwork of intermediate-type filaments, Nature 323 (1986) 560–564.
[28] E. Heitlinger, M. Peter, A. Lustig, W. Villiger, E.A. Nigg, U. Aebi, The role of the head and tail domain in lamin structure and assembly: analysis of bacterially expressed chicken lamin A and truncated B2 lamins, J. Struct. Biol. 108 (1992) 74–89.
[29] N. Stuurman, S. Heins, U. Aebi, Nuclear lamins: their structure, assembly, and interactions, J. Struct. Biol. 122 (1998) 42–66.
[30] D.A. Parry, Hendecad repeat in segment 2A and linker L2 of intermediate filament chains implies the possibility of a right-handed coiled-coil structure, J. Struct. Biol. 155 (2006) 370–374.
[31] J. Stetefeld, M. Jenny, T. Schulthess, R. Landwehr, J. Engel, R.A. Kammerer, Crystal structure of a naturally occurring parallel right-handed coiled coil tetramer, Nat. Struct. Biol. 7 (2000) 772–776.
[32] S. Ozbek, J.F. Muller, E. Figgemeier, J. Stetefeld, Favourable mediation of crystal contacts by cocoamidopropylbetaine (CAPB), Acta Crystallogr., D Biol. Crystallogr. 61 (2005) 477–480.
[33] P.B. Harbury, J.J. Plecs, B. Tidor, T. Alber, P.S. Kim, High-resolution protein design with backbone freedom, Science 282 (1998) 1462–1467.
[34] J.F. Hess, M.S. Budamagunta, R.L. Shipman, P.G. FitzGerald, J.C. Voss, Characterization of the linker 2 region in human vimentin using site-directed spin labeling and electron paramagnetic resonance, Biochemistry 45 (2006) 11737–11743.
[35] H. Bär, N. Mücke, A. Kostareva, G. Sjoberg, U. Aebi, H. Herrmann, Severe muscle disease-causing desmin mutations interfere with in vitro filament assembly at distinct stages, Proc. Natl. Acad. Sci. U. S. A. 102 (2005) 15099–15104.
[36] H. Herrmann, S.V. Strelkov, B. Feja, K.R. Rogers, M. Brettel, A. Lustig, M. Häner, D.A. Parry, P.M. Steinert, P. Burkhard, U. Aebi, The intermediate filament protein consensus motif of helix 2B: its atomic structure and contribution to assembly, J. Mol. Biol. 298 (2000) 817–832.
[37] S.V. Strelkov, J. Schumacher, P. Burkhard, U. Aebi, H. Herrmann, Crystal structure of the human lamin A coil 2B dimer: implications for the head-to-tail association of nuclear lamins, J. Mol. Biol. 343 (2004) 1067–1080.
[38] S.V. Strelkov, P. Burkhard, Analysis of alpha-helical coiled coils with the program TWISTER reveals a structural mechanism for stutter compensation, J. Struct. Biol. 137 (2002) 54–64.
[39] J.H. Brown, C. Cohen, D.A. Parry, Heptad breaks in alpha-helical coiled coils: stutters and stammers, Proteins 26 (1996) 134–145.
[40] D.A. Parry, T.A. Smith, M.A. Rogers, J. Schweizer, Human hair keratin-associated proteins: sequence regularities and structural implications, J. Struct. Biol. 155 (2006) 361–369.
[41] A.V. Sokolova, L. Kreplak, T. Wedig, N. Mücke, D.I. Svergun, H. Herrmann, U. Aebi, S.V. Strelkov, Monitoring intermediate filament assembly by small-angle X-ray scattering reveals the molecular architecture of assembly intermediates, Proc. Natl. Acad. Sci. U. S. A. 103 (2006) 16206–16211.
[42] M.E. Rafik, F. Briki, M. Burghammer, J. Doucet, In vivo formation steps of the hard alpha-keratin intermediate filament along a hair follicle: evidence for structural polymorphism, J. Struct. Biol. 154 (2006) 79–88.
[43] R.D.B. Fraser, D.A.D. Parry, Structural changes in the trichocyte intermediate filaments accompanying the transition from the reduced to the oxidized form, J. Struct. Biol. (in press), doi:10.1016/j.jsb.2007.02.001.
[44] R.D. Fraser, T.P. Macrae, Structural organization in feather keratin, J. Mol. Biol. 16 (1963) 272–280.
[45] R.D. Fraser, T.P. MacRae, A. Miller, X-ray diffraction patterns of alpha-fibrous proteins, J. Mol. Biol. 14 (1965) 432–442.
[46] W.W. Franke, D.L. Schiller, C. Grund, Protofilamentous and annular structures as intermediates during reconstitution of cytokeratin filaments in vitro, Biol. Cell 46 (1982) 257–268.
[47] H. Herrmann, T. Wedig, R.M. Porter, E.B. Lane, U. Aebi, Characterization of early assembly intermediates of recombinant human keratins, J. Struct. Biol. 137 (2002) 82–96.
[48] W. Ip, M.K. Hartzer, Y.Y. Pang, R.M. Robson, Assembly of vimentin in vitro and its implications concerning the structure of intermediate filaments, J. Mol. Biol. 183 (1985) 365–375.
[49] W. Ip, J.E. Heuser, Y.Y. Pang, M.K. Hartzer, R.M. Robson, Subunit structure of desmin and vimentin protofilaments and how they assemble into intermediate filaments, Ann. N. Y. Acad. Sci. 455 (1985) 185–199.

[50] I.A. Abumuhor, P.H. Spencer, J.A. Cohlberg, The pathway of assembly of intermediate filaments from recombinant alpha-internexin, J. Struct. Biol. 123 (1998) 187–198.
[51] H. Herrmann, U. Aebi, Intermediate filament assembly: temperature sensitivity and polymorphism, Cell. Mol. Life Sci. 55 (1999) 1416–1431.
[52] K.N., Goldie, T., Wedig, A., Mitra, U., Aebi, H., Herrmann, A. Hoenger, Dissecting the 3-D structure of vimentin intermediate filaments by cryo-electron tomography, J. Struct. Biol. (in press), doi:10.1016/j.jsb.2006.12.007.
[53] W.W. Franke, H. Zerban, C. Grund, E. Schmid, Electron microscopy of vimentin filaments and associated whisker structures in thin sections and freeze-fractures, Biol. Cell 41 (1981) 173–178.
[54] M.H. Koch, P. Vachette, D.I. Svergun, Small-angle scattering: a view on the properties, structures and structural changes of biological macromolecules in solution, Q. Rev. Biophys. 36 (2003) 147–227.
[55] M.V. Petoukhov, T.P. Monie, F.H. Allain, S. Matthews, S. Curry, D.I. Svergun, Conformation of polypyrimidine tract binding protein in solution, Structure 14 (2006) 1021–1027.
[56] T.A. Smith, P.M. Steinert, D.A. Parry, Modeling effects of mutations in coiled-coil structures: case study using epidermolysis bullosa simplex mutations in segment 1a of K5/K14 intermediate filaments, Proteins 55 (2004) 1043–1052.
[57] A. Kaminska, S.V. Strelkov, B. Goudeau, M. Olive, A. Dagvadorj, A. Fidzianska, M. Simon-Casteras, A. Shatunov, M.C. Dalakas, I. Ferrer, H. Kwiecinski, P. Vicart, L.G. Goldfarb, Small deletions disturb desmin architecture leading to breakdown of muscle cells and development of skeletal or cardioskeletal myopathy, Hum. Genet. 114 (2004) 306–313.
[58] P. Pruszczyk, A. Kostera-Pruszczyk, A. Shatunov, B. Goudeau, A. Draminska, K. Takeda, N. Sambuughin, P. Vicart, S.V. Strelkov, L.G. Goldfarb, A. Kaminska, Restrictive cardiomyopathy with atrioventricular conduction block resulting from a desmin mutation, Int. J. Cardiol. 117 (2007) 244–253.
[59] H. Bär, N. Mücke, H.A. Katus, U. Aebi, H. Herrmann, Assembly defects of desmin disease mutants carrying deletions in the alpha-helical rod domain are rescued by wild type protein, J. Struct. Biol. 158 (2007) 107–115.
[60] H. Bar, D. Fischer, B. Goudeau, R.A. Kley, C.S. Clemen, P. Vicart, H. Herrmann, M. Vorgerd, R. Schroder, Pathogenic effects of a novel heterozygous R350P desmin mutation on the assembly of desmin intermediate filaments in vivo and in vitro, Hum. Mol. Genet. 14 (2005) 1251–1260.
[61] H. Bar, N. Mucke, P. Ringler, S.A. Muller, L. Kreplak, H.A. Katus, U. Aebi, H. Herrmann, Impact of disease mutations on the desmin filament assembly process, J. Mol. Biol. 360 (2006) 1031–1042.